RSC Advances

ROYAL SOCIETY OF CHEMISTRY

www.rsc.org/advances

Graphic Abstract

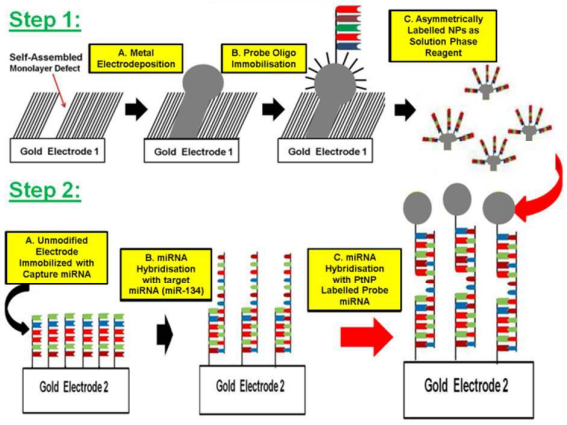

We report a novel electrochemical detection of microRNA-134, a low-abundance human plasma microRNA, based on regioselective functionalised electrocatalytic nanoparticles.

Journal Name

ARTICLE

Direct, non-amplified detection of microRNA-134 in plasma from epilepsy patients

Received 00th January 20xx,
Accepted 00th January 20xx

DOI: 10.1039/x0xx00000x

www.rsc.org/

Elaine Spain[a,b*], Eva M. Jimenez-Mateos[a], Rana Raoof[a], Hani ElNaggar[a,c], Norman Delanty[c], Robert J. Forster[b*], David C. Henshall[a*]

Biofluid-based molecular biomarkers would support clinical decision-making around diagnosis, prognosis and treatment for various diseases. MicroRNAs (miRNAs) have emerged as importa regulators of gene expression in the brain and levels of miR-134 have been found to be elevated in experimental and human epilepsy. Here we show direct detection of miR-134 in human plasma without the need for PCR amplification using platinum nanoparticles (PtNPs) that are region-selectively decorated with probe strand nucleic acids. The nanoparticles were produced by electrodeposition using nanoscale defects within self-assembled monolayers of dodecanethiol. The template breaks the symmetry of the particle allowing one side to be selectively modified with the probe and leaving the other clean and capable of catalytically reducing hydrogen peroxide. The detection electrode was functionalised with single-stranded capture miRNA, miRNA that is complementary to miR-134, but leaves a section of the target available to bind the nucleic acid sequence bound to the PtNPs. Thus, electrocatalytic nanoparticles become confined on the electrode surface only when the target is present. Significantly, the relatively large current associated with the binding of small numbers of nanoparticles and their small area of occupation leads to attomolar limits of detection and a wide dynamic range without the need for molecular, e.g., PCR amplification. Using plasma samples from health volunteers and epilepsy patients we show highly linear correlation in miR-134 measurement to results with Taqman-based PCR. The present study demonstrates rapid and simple detection of miRNA that if developed further could provide simple point-of-care devices for detection of epilepsy biomarkers.

Introduction

Biomarkers are increasingly seen as essential non-invasive tools to support diagnosis, prognosis and treatment decisions for disorders of the central nervous system.[1,2] Epilepsy is one of the most common neurological diseases. It is characterised by recurring seizures which are thought to arise from transient imbalances between excitation and inhibition in the brain.[3,4] Seizures are highly unpredictable in patients. Diagnosis is also challenging and often based on clinical examination and history alone. Electroencephalography (EEG) and brain imaging are invaluable but also costly, laborious and technically demanding. The identification of a biomarker of epilepsy in a biofluid such as blood with, ideally, a mechanistic link to the underlying pathophysiology would transform epilepsy patient care, diagnosis and prognosis.[5] Efforts to date have focused on brain proteins, autoantibodies, infective and immune molecules and have been largely unsuccessful.[5]

One promising class of biomarkers are microRNAs.[6,7] MicroRNAs (miRNAs) are 18- to 25-nucleotide small non-coding RNA molecules which function post-transcriptionally to regulate protein levels in cells.[8,9] A number of miRNA are unique to the brain, including miR-134, a miRNA with targets that control neuronal microstructure.[10,11] Recent studies reported upregulation of miR-134 in the brain in experimental and human epilepsy and showed that silencing miR-134 had long-lasting seizure-suppressive effects in mice.[12,13,14] Emerging work shows miRNA levels are also altered in the blood following seizures in rodents,[15,16,17] and in epilepsy patients.[18] Thus, analysis of the miRNA content of biofluids might provide molecular-level information to support diagnosis after a first unprovoked seizure, predict an impending seizure, provide a druggable target or monitor therapeutic efficacy.[5]

The ability to detect biomarkers of disease at ever decreasing concentrations so as to enable early detection is a major focus of contemporary sensor research. For miRNA detection, various new techniques have been reported recently, including fluorescence

[a]Department of Physiology and Medical Physics, Royal College of Surgeons in Ireland, Dublin 2, Ireland
[b]School of Chemical Sciences, National Centre for Sensor Research, Dublin City University,
Dublin 9, Ireland
[c]Neurological Services, Beaumont Hospital, Dublin 9, Ireland
† Footnotes relating to the title and/or authors should appear here.
Electronic Supplementary Information (ESI) available: [details of any supplementary information available should be included here]. See DOI: 10.1039/x0xx00000x

colorimetry,[21] surface plasmon resonance (SPR),[20,21] and electrochemistry.[22] Electrochemical biosensors have attracted increasing attention due to advantages such as simplicity, portability, sensitivity, responsivity and low-cost, and hold promise as devices suitable for point-of-care diagnostics.[23] One of the biggest challenges for the development of miRNA sensors is the limit of detection, since the miRNA concentration is attomolar to femtomolar in biological samples.[20] Thus, a 100 µl sample of a patient's blood may contain less than 10000 copies of one of these biomarkers. Moreover, these disease biomarkers must be detected in the presence of thousands of proteins and other nucleic acids that have the potential to interfere with the analysis. These extreme demands of sensitivity and selectivity mean that methods typically rely on an initial amplification step, e.g., PCR or nucleic acid sequence-base amplification (NASBA). To date, there are several reviews available which are based on the advancement of sensitive electrochemical biosensors and immunosensors and the great benefits of incorporating different nanomaterials into the main design for the detection of low-abundance miRNAs [20,21,22,24] For example, Zuo *et al*[25] demonstrated an ultrasensitive detection platform for miRNA by combining hybridization chain reaction (HCR) amplification and the tetrahedral DNA nanostructure probes. However this technology includes multiple steps and specialised equipment. The state-of-the-art in the field of microfluidic detection of miRNA expression profiles is dominated by devices that amplify the target rather than the direct detection approach reported here in which the signal generated by the hybridisation of the few copies of the target is massively amplified by electrocatalysis.

Here we report the use of electrocatalytic metal nanoparticles that are functionalised with probe strand nucleic acids that are complementary to the target in just one region to detect miR-134 directly in undiluted patient serum at sub-femtomolar concentrations without PCR amplification of the target (Scheme 1). The approach is based on regioselective, hemi-spherical platinum nanoparticles,[20-22] that are deposited within defects of a self-assembled monolayer. This strategy allows the top surface of these PtNPs to be selectively functionalized with thiol terminated probe strand miRNA. This method has the advantage of controlling the density and orientation of probe miRNA on the surface of the PtNPs, which is usually quite challenging in electrochemical biosensors. Applying a current step causes rapid desorption of the functionalized PtNPs. These DNA labelled electrocatalytic particles are then used in a sandwich assay to determine the concentration of the target by measuring the faradaic current associated with reduction of peroxide in solution. These particles are capable of detecting miR-134 in clean buffer and patient samples with high sensitivity and selectivity.

Experimental

Materials

Dodecanethiol, Denhardt's hybridization solution (≥99.5%), for miRNA probe assembly and Chloroplatinic acid hydrate (H_2PtCl_6, 99.995%) were used as received from Sigma-Aldrich. All aqueous solutions were prepared using RNase free water. The oligonucleotides were purchased from Eurogenec and their purity was >98%. The base sequences are as follows: Capture: 5'-ACC-AGU-CAC-A-3'- SH; Target: 5'-UGU-GAC-UGG-UUG-ACC-AGA-GGG-G-3'; Probe: SH-5'-CCC-CUC-UGG-U-3'

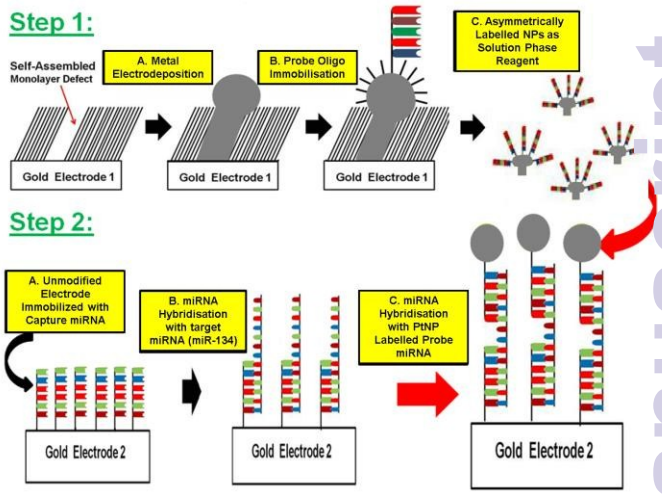

Scheme 1. Platinum nanoparticle formation and regio-selective miRNA functionalisation.

Instrumentation

A three-electrode electrochemical cell was used at a temperature of 22 ± 2°C. The working electrode was a 2 mm diameter planar gold disc. It was polished with a nylon cloth with 1 µm diamond polish and thoroughly rinsed with Milli-Q water and ethanol before sonication in Milli-Q water for 5 minutes. Voltammetry in 0.1 M H_2SO_4 was used to determine the surface roughness factor by scanning the electrode between +1.500 and -0.300 V. The counter electrode was a large area coiled platinum wire and a silver/silver chloride (Ag/AgCl in 3 M KCl) acted as reference. Dynamic Light Scattering (DLS) was performed at 25°C on a Nanosizer NanoZS (Malvern Instruments, Malvern U.K.) using a detection angle of 173° and a 3 mW He–Ne laser was operating at a wavelength of 633 nm. The d_{hyd} values reported are the Z-average diameters (mean hydrodynamic diameter based upon the intensity of scattered light). The polydispersity indices were also calculated from the Cumulants analysis as defined in ISO13321. The intensity size distributions were obtained from analysis of the correlation functions using the Multiple Narrow Modes algorithm based upon a non-negative least-squares fit,[26] using Dispersion Technology software (v. 5.3, Malvern Instruments; Worcestershire, U.K.). The values used for the viscosity of 0.01 M H_2SO_4 was 26.7 cPa·s at 298 K. Scanning electron microscopy was performed using a Hitachi S-3400N scanning electron microscope. EDX measurements were performed using an Oxford INCA microanalysis system using an X-Max detection system.

Human plasma samples

Studies were approved by the Research Ethics Committee of the Royal College of Surgeons in Ireland (REC #859) and by the Ethics (Medical Research) Committee of Beaumont Hospital, Dublin. Informed written consent was obtained from all patients and volunteers. Blood was collected by venupuncture into K2-EDTA tube, 10 ml, BD cat. no. 367525, gently inverted 8 – 10 times, and processed to obtain plasma within one hour. After centrifugation, samples were decanted for storage in a cryo-tube (Greiner Bio-one) and frozen at -80°C. Prior to RNA extraction, frozen plasma was processed a second time by centrifugation at 1940 x g to minimize potential cellular contaminants.[27]

Table 1. Summary of patient and healthy volunteer data
Key: F, female; M, male; y, years; TLE, temporal lobe epilepsy; JME, juvenile myoclonic epilepsy; LEV, levetiracetam; LAC, lacosamide; PER, perampanel; CBZ, carbamazepine; TPN, topiramate; GABA, gabapentin; ZNS, zonisamide; PHY, phenytoin.

Patient	Age	Sex	Epilepsy syndrome	Aetiology	Epilepsy duration	AED
A	43	F	Localisation-related epilepsy (TLE)	None/unknown	12 years	LEV, LAC
B	21	M	Localisation-related epilepsy (TLE)	Febrile Convulsions	16 years	VAP
C	21	F	Idiopathic Generalised Epilepsy (JME)	Likely genetic with strong family history	18 years	LAC, ZNS, PHY, PER
D	59	F	Localisation-related epilepsy (TLE)	None/unknown	42 years	CBZ, TPN, GABA
E	18	F	Localisation-related epilepsy (TLE)	Right Occipito-Parietal Gliosis with associated volume loss	8 years	LEV, LAC, PER
F	43	F	Localisation-related epilepsy (TLE)	Febrile Convulsions	37 years	CBZ, TPN
G	35	M	-	-	-	-
H	46	M	-	-	-	-

Patients
Plasma was obtained from two (2) healthy volunteers (Male; 35, 46 y) and six (6) patients with epilepsy. Patient data are presented in Table 1. All patients had been referred for video-EEG monitoring at Beaumont hospital for refractory epilepsy. All patients were on medication at the time of the study. Blood samples were collected with a confirmed seizure-free monitoring period of at least 24 h.

RNA extraction and qPCR
RNA was extracted from 200 µl of plasma using the miRCURY biofluids kit (Exiqon, Denmark), following manufacturer's instructions. Levels of miRNA-134 were analyzed using the small-scale RT-PCR protocol.[28] Briefly, a fixed volume of input RNA (1.67 ml) was reverse transcribed using the *Taq*Man miRNA Reverse

Transcription Kit and miRNA134-specific stem-loop primers (Applied BioSystems) in a small-scale RT reaction (containing per sample 1.387ml of H_2O, 0.5 ml of 10X Reverse-Transcription Buffer, 0.063 ml of RNase-Inhibitor, 0.05 ml of 100 mM dNTPs and 0.33 ml of Multiscribe Reverse Transcriptase). 2.25 ml of diluted RT product (prepared by combining 5.0 ml of RT product with 28.4 ml of H_2O) was combined with 2.75 ml of PCR assay reagents (2.5 ml of TaqMan 2X Universal PCR Master Mix and 0.25 ml of TaqMan miRNA Assay). Real time qPCR was carried out on a 12K Flex Quant-Studio PCR system and Ct values were correlated with mA data.

Monolayer self-assembly
The gold electrodes were cleaned by placing them in piranha solution (3:1 mixture of sulphuric acid and 30% hydrogen peroxide) for 20 min, followed by thorough rinsing with ultrapure water. The electrode was then scanned between +1.500 and -0.300 V in 0.01 M H_2SO_4 to measure the surface roughness of the gold electrode. The gold disk electrode was then washed with ethanol and placed in a 1 mM solution of dodecanethiol in ethanol and monolayer self-assembly allowed to proceed for 7 hours. After the formation of the incomplete monolayer, the substrate was rinsed with ethanol and dried under a N_2 stream.

miRNA probe immobilization and hybridization: Fabrication of region-selectively miRNA functionalized platinum nanoparticles
Platinum nanoparticles were electrodeposited from 1 mM hydrogen hexachlorideplatinate(IV) hydrate (H_2PtCl_6) in 0.5 M H_2SO_4 using the defects within the self-assembled monolayer as templates. Subsequently, the PtNPs were functionalized with probe oligo (5' thiolate) by immersing the nanoparticle functionalized electrode in a 1 µM solution of the probe oligo strand dissolved in Denhardt's buffer for 2 h. The modified electrodes were then washed with RNase-free water for 15 seconds to remove loosely bound oligo and immersed in 0.01 M H_2SO_4. The oligo functionalized platinum nanoparticles were then desorbed by applying a current of +0.01 A (reductive) for 120 seconds.

A monolayer of capture strand miRNA was prepared on a freshly polished and electrochemically cleaned gold disk electrode by immersing it in a 10 µM solution of the capture strand miRNA dissolved in Denhardt's Buffer. After 5 h, the electrode was rinsed with RNase free water for 15 seconds to remove loosely bound oligo. Hybridization of the target at concentrations between 1 aM and 1 µM to the immobilized capture strand was performed at 37 ºC in Denhardt's Buffer for 90 min. Following hybridization, the modified electrode was rinsed thoroughly with buffer.

The nanoparticle labelled probe miRNA was then hybridized to the complementary section of the target not used for binding to the capture strand for 2 h at 37°C in Denhardt's Buffer. Finally, before quantitation, it was thoroughly washed with RNase free water. Following assembly of the capture-target-nanoparticle labeled probe miRNA sequence, the modified electrode was placed in an aqueous solution of 0.01 M H_2SO_4 and the current measured at -0.250 V after equilibration for 10 minutes. Then, sufficient hydrogen peroxide added to give a final concentration of 200 µM and the current associated with peroxide reduction at the bound PtNPs measured at -0.250 V after 10 minutes. The analytical response is taken as the difference in current, Δi, measured before and after peroxide addition.

Results and discussion

Template formation and nanoparticle deposition
The platinum nanoparticles perform two functions in this assay. First, they carry a high concentration of the nucleic acid strand that is complementary to the target enhancing the labelling efficiency of the target. Second, they need to generate a large, stable electrocatalytic current. Electrocatalysis occurs most efficiently at clean, unmodified surfaces and would be inhibited by the presence of immobilised probe strands. To address this issue, we used defects within a self-assembled monolayer as templates to enhance the size monodispersity of the particles and to allow one side of the nanoparticles to be functionalised. By creating "mushroom" shaped particles, the template also facilitates desorption of the nanoparticles. Here, an alkane-thiol monolayer has been deposited onto 2 mm radius gold electrodes for 7 h to create a film that contains nanoscale defects into which platinum nanoparticles can be electrodeposited. Figure 1 (A) and (B) shows typical voltammograms in sulphuric acid for a 2 mm radius gold electrode before and after deposition of the defective monolayer, respectively. By comparing the charge passed under the gold oxide reduction peak centred at approximately +0.8 V before and after monolayer deposition, the area available for PtNP electrodeposition

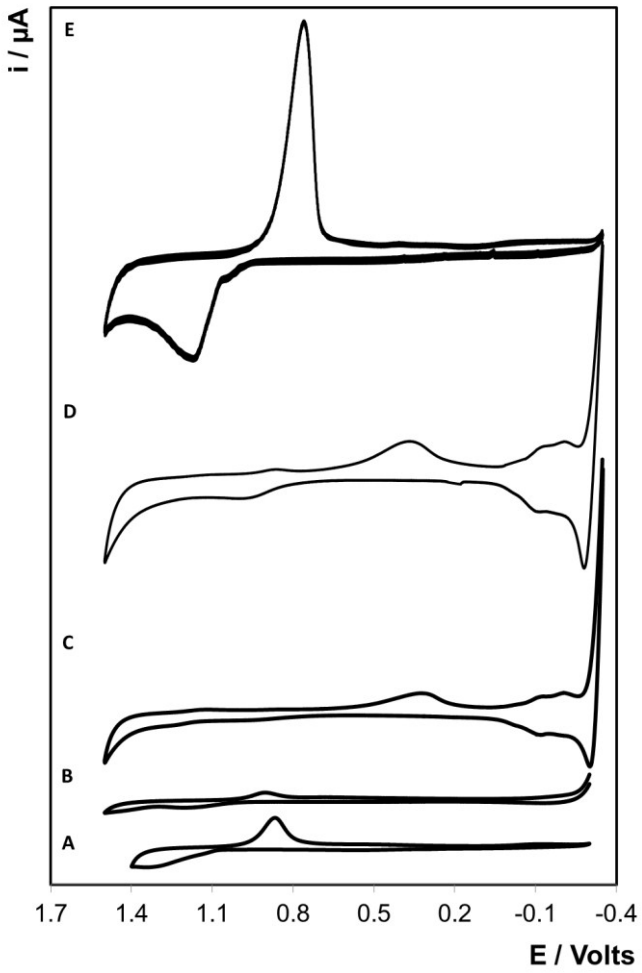

Figure 1. Cyclic voltammograms of: (A) 2 mm unmodified gold electrode, (B) after deposition of a defective C_{12} monolayer, (C) following electrodeposition of platinum nanoparticles into the monolayer defects and (D) hybridisation of Probe miRNA and (E) after the platinum nanoparticles have been desorbed. The scale bar for (A) and (B) are 10 µA, for (C) and (D) are 5 µA while for (D) and (E) it is 50 µA. In all cases the supporting electrolyte was 0.1 M H_2SO_4, the counter electrode was a large area platinum wire and the reference electrode was a saturated Ag/AgCl (3 M KCl). The scan rate is 100mVs^{-1}. The voltammograms have been displaced vertically for clarity of presentation

can be determined. This figure reveals that the area decreases by approximately 50% following monolayer deposition for 7 h, from the value of 0.035 cm^2 found for the unmodified electrode (roughness factor of 1.1) to 0.028 cm^2. Platinum nanoparticles were deposited into the defects within the monolayer from a 0.5 M sulphuric acid solution containing 1 mM hydrogen hexachlorideplatinate (IV) hydrate (H_2PtCl_6) at -0.250 V for 180 s. Figure 1(C) reveals that the microscopic area following nanoparticle deposition is 0.195 ± 0.05 cm^2, i.e., nanoparticle deposition increases the area available for miRNA deposition by a factor of approximately 9 compared to the dodecanethiol templated electrode, i.e., the PtNPs are definitely mushroom shaped. This particle shape will result in approximately two thirds of the total nanoparticle surface (hemisphere) being modified by probe strand DNA with at least one third (disk) being unmodified and available for efficient electrocatalysis. Significantly, after electrodeposition of Pt, the peak associated with gold oxide formation and reduction disappears, indicating that the defects within the monolayer have been successfully filled with platinum. The reduction of platinum oxide to metallic platinum is observed at around 0.305 V and the peak at approximately -0.258 V is attributed to hydrogen adsorption/desorption from the platinum nanoparticle surface. After the hybridisation of the probe oligo, Figure 1(D), the area decreases by approximately 8%, from the value of 0.195 cm^2 found for the nanoparticle modified electrode (roughness factor of 6.2) to 0.179 cm^2, indication that the nanoparticle functionalized electrode has undergone thiolated probe strand hybridization. A short current pulse at a current density of approximately +100 mA cm^{-2} was applied to the nanoparticle modified electrode following immobilisation of the probe oligo, with the objective of breaking the nanowire connecting the hemispherical nanoparticle to the electrode. This current jump rapidly desorbs the functionalised nanoparticles into solution minimizing the opportunity for damage to the bound miRNA. The effect of PtNP desorption from the electrode surface is highlighted in Figure 1(E), with an apparent decrease in peak height in both the reduction and oxidation proce for the platinum oxide peaks. Concurrently, a peak corresponding to gold oxide peak reduction is observed following PtNP desorptic The gold oxide peak is considerably larger than that found for the dodecanethiol templated electrode suggesting that the current step not only removes the platinum nanoparticles but also the templating alkane thiol monolayer.

Morphological and composition characterisation

Figure 2(A) shows an SEM image of the desorbed nanoparticles that have been dropcast onto a gold sheet. Based on analysis of more than 500 individual particles, their radius is 100 ± 60 nm. This image also demonstrates that a relatively high concentration of nanoparticles can be achieved in suspension. Figure 2(B) illustrates the size distribution as determined by DLS. In agreement with the SEM, the nanoparticles had an average radius of 80 ± 40 nm. Figure 2(C) shows that the energy dispersive X-ray (EDX) obtained from the suspended nanoparticles is dominated by elemental platinum with high purity.

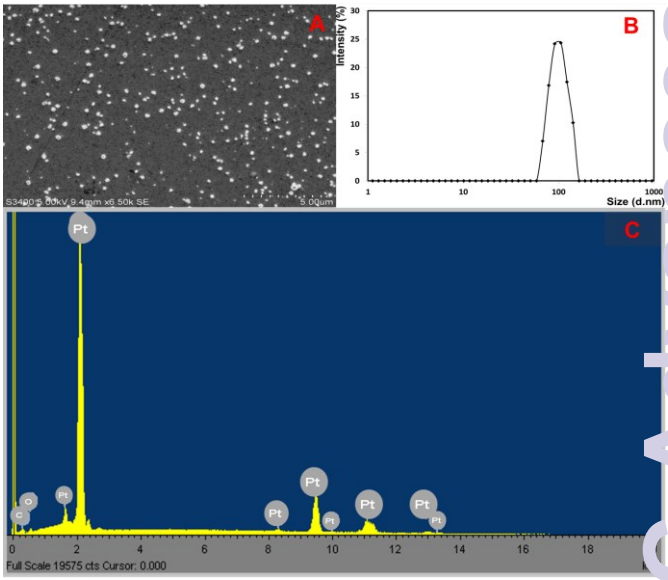

Figure 2. (A) Drop cast film of desorbed nanoparticles from suspension. The acceleration voltage is 5 kV. (B) DLS particle size distributions and (C) Energy dispersive X-ray spectrum for the desorbed platinum nanoparticles.

Nucleic Acid Mediated Nanoparticle Immobilisation

As illustrated in Scheme 1, a pristine electrode modified with miRNA capture oligos was allowed to first hybridize with different concentrations of the miR-134 target, part of which is complementary to the capture strand. This electrode was then placed into the PtNP suspension for 90 min during which time the free section of the target hybridizes with the oligo bound to the metal nanoparticle. Figure 3 shows the voltammogram obtained for a pristine gold electrode modified with capture strand miRNA after both the target miR-134 and nanoparticle functionalized probe strand hybridization steps have occurred. Significantly, oxide formation on the platinum nanoparticles is observed at potentials positive of approximately +1.100 V, the corresponding reduction

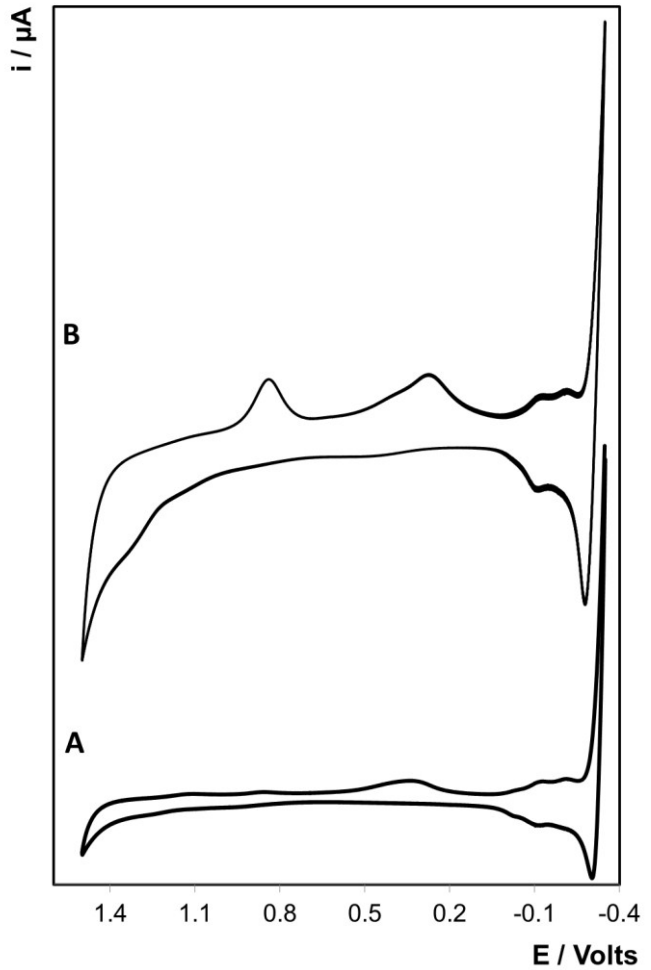

Figure 3. Cyclic voltammogram of a 2 mm radius gold disc electrode after modification with capture strand miRNA (A) and hybridization with the target and nanoparticle labelled probe sequence (B) where the miR-134 target strand concentration is 1 µM. The supporting electrolyte is 0.01 M H_2SO_4 and the scan rate is 100 mV s^{-1}.

occurs at approximately +0.2 V and hydrogen adsorption/desorption is seen between -0.05 V and -0.35 V. These observations indicate successful binding of the nanoparticles. Significantly, control experiments in which platinum nanoparticles functionalized with probe strand DNA are exposed to freshly polished gold electrodes, i.e., there is no immobilised capture strand, do not exhibit any measurable peaks associated with platinum oxide formation or reduction. This result suggests that nonspecific binding of the platinum nanoparticles is not a significant issue.

Detection of miR-134 in clean buffer

Platinum nanoparticles are well-known to be highly catalytic for the reduction of hydrogen peroxide so the response associated with target hybridisation is greatly amplified. The current associated with the reduction of H_2O_2 at the surface of the PtNPs depends on the number of PtNPs on the surface of the electrode, which depends on the concentration of target miRNA. Here, a fixed potential of -0.250 V was applied to the working electrode and the difference in the current observed in the absence of any deliberately added peroxide and after the addition of 200 µM H_2O_2, to the cell, Δi, was measured. The system was allowed to equilibrate for ten minutes following peroxide addition.

Figure 4 shows the dependence of Δi on log [miRNA] where the probe strand is unlabelled and where the PtNP label is regi selectively modified with probe strand miRNA. As expected, where the probe strand is not labelled, its hybridization with the targ does not produce any significant additional current. The low currents observed in the absence of PtNPs indicate that the

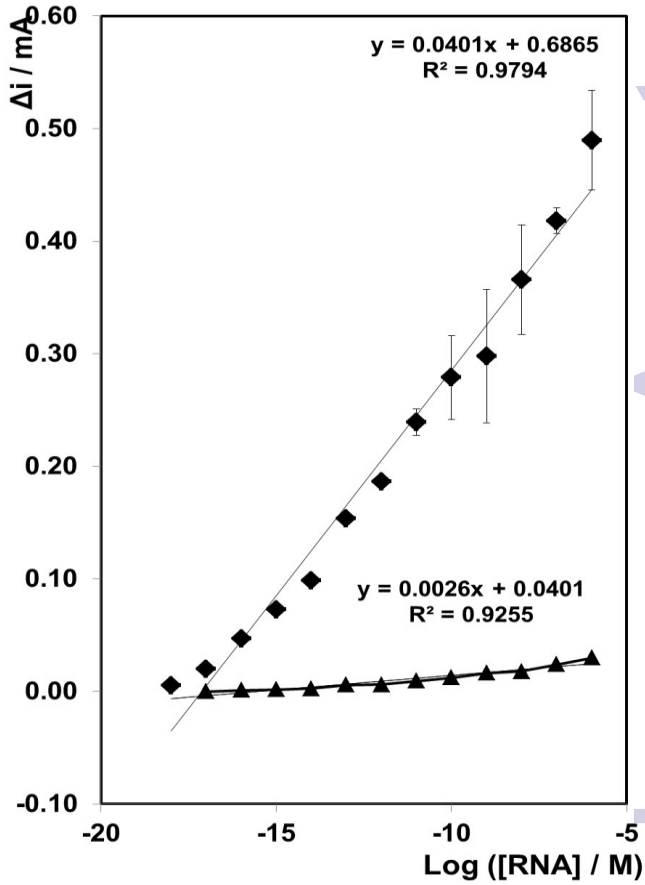

Figure 4. Dependence of the difference in current before and aft addition of H_2O_2 on log[DNA] for a 2 mm diameter bare electrode following hybridization with probe DNA that is labelled with PtNPs (♦) and where the probe is unlabelled(▲) (n=3). In both cases, th solution contains 2 mM H_2O_2 in aqueous 0.01 M H_2SO_4. Δi represents the difference in current before and after addition of the H_2O_2 at an applied potential of −0.250 V. Where error bars are not visible, they are smaller than or comparable to, the size of the symbols and range from 1.1% to 3.5%.

background current associated with direct reduction of hydrogen peroxide at the underlying electrode is low. This result is significant as it is the signal-to-noise ratio that dictates the limit of detection that can be achieved. For the full sandwich assay, an acceptably linear response (R^2 = 0.9794) is observed for concentrations of miR-134 from 1 aM to 1 μM. The absolute currents observed are in the hundreds of microamp range indicating significant electrolysis of the hydrogen peroxide. These relatively large currents suggest that heterogeneous electron transfer from the platinum nanoparticles, through the DNA linker, to the underlying electrode is relatively facile. Moreover, because nanoparticles are used as electrocatalytic labels, the rate of mass transport of H_2O_2 is likely to be enhanced relative to a planar electrode due to radial diffusion. The wide dynamic range, more than nine orders of magnitude, arises because the area of occupation of an individual nanoparticle is small and even for high concentrations sufficient area is available on the electrode to accommodate additional particles.

The Limit of Detection, LOD, is determined by utilising both the measured Limit of Blank, LOB, and test replicates of a sample known to contain a low concentration of analyte;

LOD = LOB + 1.645(Std. Dev. low concentration sample) **Eq. 1**

While the ability of the assay to detect the actual concentration has not been demonstrated, the LOD defined as the lowest analyte concentration likely to be reliably distinguished from LOB and at which detection is feasible is calculated to be 0.0263 aM

Detection of miR-134 in epilepsy patient plasma

Finally, we sought to assess the performance of the electrochemical sensor at detecting miR-134 in human plasma samples and compare this to standard Taqman PCR-based measurement. Levels of miR-134 are normally very low in human plasma. A recent study, for example, reported plasma miR-134 at C_t 31 using Taqman low-density array qRT-PCR profiling.[28] This is consistent with miR-134 being a brain-restricted miRNA.[10] This makes it particularly well-suited to assaying here in order to demonstrate sensitivity of the electrochemical sensor to detect low-abundance miRNAs. Although miR-134 levels are increased in the brain in experimental and human epilepsy, it is unknown if of miR-134 are altered in patient plasma.

In the present studies, plasma was obtained from health volunteers and from patients with drug-refractory epilepsy during in-patient care (video-EEG monitoring) (see Table 1). Blood samples were collected and processed for plasma followed by RNA extraction. The extracted RNA was then analysed either using the electrochemical sensor or processed for real-time PCR analysis using a standard Taqman miRNA assay for miR-134. As expected, the Taqman miRNA assay detected very low levels of miR-134 in the samples from healthy volunteers (Ct range 29-33, Figure 5). These values fall within the range reported by others using PCR-based detection of miR-134 in healthy volunteer plasma.[27] In contrast, plasma levels of miR-134 measured by Taqman miRNA assay were consistently higher in the epilepsy patient plasma (Figure 5). Measurement of miR-134 in the same set of samples using the PtNP produced a highly linear correlation to the Taqman assay, with R^2 = 0.95. These data demonstrate the electrochemical sensor provides highly sensitive detection of miR-134 in human plasma and suggests miR-134 levels may be increased in patients with refractory

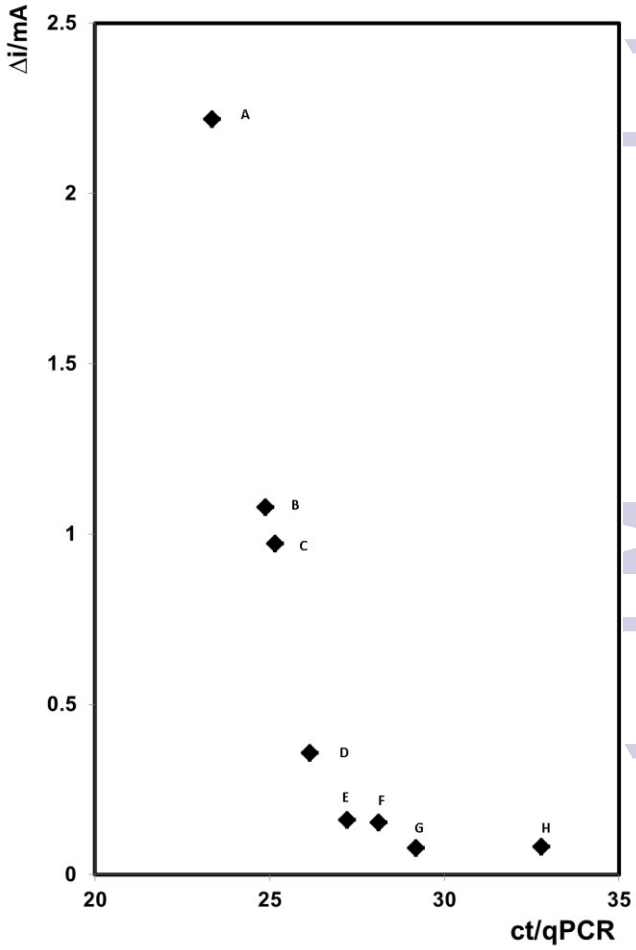

Figure 5. Comparison of miRNA detection with real-time PCR
Graph shows plots of readings from individual samples of RNA extracted from plasma, plotting the Δi against real-time PCR cycl (Ct) value. All clinical data of patient and healthy volunteer data is given in Table 1.

epilepsy. A poorer correlation was observed in the comparison of the system to the Taqman miRNA assay at the lowest levels of miRNA detection (e.g. samples from healthy controls G, H). This may be due to the sensitivity of the Taqman assay. While CT values correlate to the RNA input for miRNA assays over four orders of magnitude,[29] the control samples with Ct values close or above 30 may contain 10 or less copies of miRNA and measurement of these very low abundance miRNAs by Taqman assay becomes less reliable. Regarding the selectivity of the sensor, the structure of miR-758 is the most similar to miR-134 and contains a sequence of 14 bases that are the same as that found in miR-134. However, we have previously demonstrated[30,31,32] that in an assay of this kind th electrocatalytic current observed decreases by approximately a factor of 4 when there is only 1 base mismatches present. Therefore, the current response observed will be dominated b miR-134. Equally, the electrocatalytic reaction causes any non-specifically bound protein to be desorbed from the nanoparticle surface making the response insensitive to non-specific binding.

Conclusions

Platinum nanoparticles that are regio-selectively functionalized (upper surface only) with probe strand miRNA while the remainder

of the particles surface remains clean, generate significant electrocatalytic currents when immobilised on an electrode surface in a nucleic acid sandwich assay. A key advantage of desorbing these particles is that they can quickly sample the solution for target miRNA by stirring rather than waiting for target strands to arrive at the electrode interface. This is particularly important for low, i.e., aM concentrations, where diffusion is too slow to allow the surface coverage of the target to reach equilibrium on a meaningful timescale. The assay is characterized by a wide dynamic range (more than eight orders of magnitude), high sensitivity and a calculated LOD of 0.0263 aM (lowest analyte concentration likely to be reliably distinguished from LOB and at which detection is feasible). While it is not possible to detect the arrival of single particles it is perhaps important to note that the rather poor size monodispersity (80 +/- 40nm) may compromise the reproducibility for the lowest concentrations of miRNA investigated. Significantly, we were able to demonstrate the ability to detect a low-abundance miRNA linked to epilepsy using human plasma. Emerging data show miR-134 is upregulated in the brain in experimental and human epilepsy and while miRNA biomarkers of epilepsy have been reported,[18, 19] the present study is the first to provide evidence that miR-134 is increased in plasma from epilepsy patients. Here we show that the electrochemical sensor PtNP-based miR-134 detection is highly correlated with Taqman-based measurement of plasma miR-134 levels, validating the method.

In summary, the present study demonstrates a novel electrochemical detection based on regioselective functionalised electrocatalytic nanoparticle suitable for the detection of low-abundance molecular biomarkers of disease and suggests plasma miR-134 may be a biomarker of refractory epilepsy.

Acknowledgements

This material is based upon works supported by the IRC under Project No. GOIPD/2014/416, by Science Foundation Ireland under Grant No. 10/IN.1/B3121 and 13/IA/1891 and by funding from the European Union's Seventh Framework Programme (FP7/2007-2013) under grant agreement no. 602130.

Notes and references

[1] H. Hampel, R. Frank, K. Broich, S. J. Teipel, R. G. Katz, J. Hardy, K. Herholz, A. L. Bokde, F. Jessen, Y. C. Hoessler, W. R. Sanhai, H. Zetterberg, J. Woodcock and K. Blennow, *Nature reviews. Drug discovery*, 2010, **9**, 560-574.

[2] H. Zetterberg, D. H. Smith and K. Blennow, *Nature reviews. Neurology*, 2013, **9**, 201-210..

[3] R. S. Fisher, C. Acevedo, A. Arzimanoglou, A. Bogacz, J. H. Cross, C. E. Elger, J. Engel, Jr., L. Forsgren, J. A. French, M. Glynn, D. C. Hesdorffer, B. I. Lee, G. W. Mathern, S. L. Moshe, E. Perucca, I. E. Scheffer, T. Tomson, M. Watanabe and S. Wiebe, Epilepsia, 2014, 55, 475-482.

[4] B. S. Chang and D. H. Lowenstein, *The New England journal of medicine*, 2003, **349**, 1257-1266.

[5] M. Hegde and D. H. Lowenstein, *Biomarkers in medicine*, 2014, **8**, 413-427.

[6] P. Rao, E. Benito and A. Fischer, *Frontiers in molecular neuroscience*, 2013, **6**, 39.

[7] D. C. Henshall, *Current opinion in neurology*, 2014, **27**, 199-205

[8] M. R. Fabian, N. Sonenberg and W. Filipowicz, *Annual review of biochemistry*, 2010, **79**, 351-379.

[9] H. I. Im and P. J. Kenny, *Trends in neurosciences*, 2012, **35**, 325-334.

[10] G. M. Schratt, F. Tuebing, E. A. Nigh, C. G. Kane, M. E. Sabatini, M. Kiebler and M. E. Greenberg, *Nature*, 2006, **439**, 283-289.

[11] R. Fiore, S. Khudayberdiev, M. Christensen, G. Siegel, S. W. Flavell, T. K. Kim, M. E. Greenberg and G. Schratt, *The EMBO journal*, 2009, **28**, 697-710.

[12] E. M. Jimenez-Mateos, T. Engel, P. Merino-Serrais, R. C. McKiernan, K. Tanaka, G. Mouri, T. Sano, C. O'Tuathaigh, J. L. Waddington, S. Prenter, N. Delanty, M. A. Farrell, D. F. O'Brien, R. M. Conroy, R. L. Stallings, J. Defelipe and D. C. Henshall, *Nature medicine*, 2012, **18**, 1087-1094.

[13] J. Peng, A. Omran, M. U. Ashhab, H. Kong, N. Gan, F. He and F. Yin, *J Mol Neurosci*, 2013, **50**, 291-297.

[14] E. M. Jimenez-Mateos, T. Engel, P. Merino-Serrais, I. Fernaud-Espinosa, N. Rodriguez-Alvarez, J. Reynolds, C. R. Reschke, R. M. Conroy, R. C. McKiernan, J. deFelipe and D. C. Henshall, *Brain structure & function*, 2015, **220**, 2387-2399.

[15] J. A. Gorter, A. Iyer, I. White, A. Colzi, E. van Vliet, S. Sisodiya and E. Aronica, *Neurobiology of disease*, 2013, DOI: S0969-9961(13)00301-X [pii]10.1016/j.nbd.2013.10.026.

[16] D. Z. Liu, Y. Tian, B. P. Ander, H. Xu, B. S. Stamova, X. Zhan, R. J. Turner, G. Jickling and F. R. Sharp, *Journal of cerebral blood flow and metabolism : official journal of the International Society of Cerebral Blood Flow and Metabolism*, 2010, **30**, 92-101.

[17] K. Hu, C. Zhang, L. Long, X. Long, L. Feng, Y. Li and B. Xiao, Neuroscience letters, 2011, 488, 252-257.

[18] J. Wang, J. T. Yu, L. Tan, Y. Tian, J. Ma, C. C. Tan, H. F. Wang, Y. Liu, M. S. Tan, T. Jiang and L. Tan, *Scientific reports*, 2015, **5**, 9522.

[19] J. Wang, L. Tan, L. Tan, Y. Tian, J. Ma, C. C. Tan, H. F. Wang, Y. Liu, M. S. Tan, T. Jiang and J. T. Yu, *Scientific reports*, 2015, **5**, 10201.

[20] L. Yang, C. Liu, W. Ren and Z. Li, *ACS applied materials & interfaces*, 2012, **4**, 6450-6453.

[21] E. Hamidi-Asl, I. Palchetti, E. Hasheminejad and M. Mascini, *Talanta*, 2013, **115**, 74-83.

[22] L. Liu, N. Xia, H. Liu, X. Kang, X. Liu, C. Xue and X. He, *Biosensors & bioelectronics*, 2014, **53**, 399-405.

[23] E. Palecek and M. Bartosik, *Chemical reviews*, 2012, **112**, 3427-3481.

[24] L. O'Connor and B. Glynn, *Expert review of medical devices*, 2010, **7**, 529-539.

[25] Zhilei Ge, Meihua Lin, Ping Wang, Hao Pei, Juan Yan, Jiye Shi, Qing Huang, Dannong He, Chunhai Fan, and Xiaolei Zuo Anal. Chem., 2014, **86,** 2124–2130.

[26] C. L. Lawson and R. J. Hanson, *Solving Least Squares Problems*, Society for Industrial and Applied Mathematics, 1974.

[27] H. H. Cheng, H. S. Yi, Y. Kim, E. M. Kroh, J. W. Chien, K. D. Eaton, M. T. Goodman, J. F. Tait, M. Tewari and C. C. Pritchard, *PloS one*, 2013, **8**, e64795.

[28] P. S. Mitchell, R. K. Parkin, E. M. Kroh, B. R. Fritz, S. K. Wyman, E. L. Pogosova-Agadjanyan, A. Peterson, J. Noteboom, K. C. O'Briant, A. Allen, D. W. Lin, N. Urban, C. W. Drescher, B. S. Knudsen, D. L. Stirewalt, R. Gentleman, R. L. Vessella, P. S. Nelson, D. B. Martin and M. Tewari, *Proceedings of the National Academy of Sciences of the United States of America*, 2008, **105**, 10513-10518.

[29] C.F. Chen, D.A. Ridzon, A.J. Broomer, AJ; et al. *Nucleic Acid research*, 2005, **33**, e179.

[30] E Spain, E Brennan, H McArdle, T.E. Keyes, and R.J. Forster, *Analytical Chemistry*, 2012, **84**, 6471−6476.

[31] E Spain, H McArdle, T.E. Keyes and R.J. Forster, *Analyst*, 2013, **138**, 4340–4344.

[32] E Spain, E Brennan, T.E. Keyes and R.J. Forster, *Electrochimica Acta*, 2014, **128**, 61–66.